The Journal of Chemical Physics

AIP Publishing

Heterogeneous dynamics in aging phosphate-based geopolymer

Alberto Viani [1a], Davide Bernasconi [2], Lucie Zárybnická [3], Federico Zontone [4], Alessandro Pavese[2], Francesco Dallari [3]

[1] *Department of Chemical and Geological Sciences, University of Modena and Reggio Emilia, 41125 Modena, Italy*

[2] *Earth Sciences Department, University of Turin, 10125 Turin, Italy*

[3] *Institute of Theoretical and Applied Mechanics of the Czech Academy of Sciences, Centre Telč, 58856 Telč, Czech Republic*

[4] *European Synchrotron Radiation Facility, 38043 Grenoble, France*

[5] *Department of Physics and Astronomy 'Galileo Galilei', University of Padova, 35131 Padova, Italy*

[a)] Author to whom correspondence should be addressed: alberto.viani@unimore.it

Abstract

The time-evolution of dynamics, microstructure and mechanical response of phosphate-based geopolymers was probed using X-ray photon correlation spectroscopy and rheological tests. The analyzed relaxation processes in the freshly prepared geopolymer mixes evidenced a *q*-independent mode of the autocorrelation function, ascribed to density fluctuations of the already established molecular network, undergoing reconfiguration without significant mass transport. Upon curing, the detected motions are localized and depict a system evolving towards structural arrest dominated by slower hyperdiffusive dynamics, characterized by a compressed exponential regime, pointing to a structural relaxation process subjected to internal stresses, in a context of marked dynamical and structural heterogeneity.

The system ages through a 'densification' process producing a declining small angle scattered intensity, as two finely intermixed gel-like reaction products, namely, one hydrated aluminophosphate and one hydrated silica, form a percolated network possessing surface fractal

scaling of progressively shorter average correlation length. In this scenario, the nominal Al/P molar ratio of the mix, being an index of network-forming ability, is positively correlated with the dynamic viscosity and the overall kinetics, whereas the contrary occurs for the fraction of water.

I. Introduction

Inorganic polymers exhibiting cohesive properties are of interest for a number of applications (e.g., inorganic foams, structural cements, matrices for waste encapsulation, refractory materials, coatings, and bioceramics) because of their excellent chemical and thermal stability and good mechanical performance [1–3]. Phosphate-based geopolymers (PBGs), alternatively known as phosphoric acid-based geopolymers, silico-aluminophosphate geopolymers or chemically-bonded phosphates, form by the reaction of a solution of phosphoric acid with an aluminosilicate source (e.g., calcined clay) [4]. It is generally accepted that the formation of PBGs starts with the dissolution of the aluminosilicate source in the acidic environment. The released Al^{3+} ions poly-condense with the phosphate anions into an aluminophosphate hydrogel network [1,2]. Information about the reaction mechanisms and structural details of the material is still incomplete because of the number of variables influencing the reaction path, such as the concentration and amount of acid solution, the nature and characteristics of the aluminosilicate source (e.g., powder fineness and calcination temperature), and the presence of additional ions in the solution [5–8]. However, such information is of crucial interest in order to tune the properties in view of the potential applications of the material.

In a series of experiments, the progressive dilution of the concentrated phosphoric acid solution was found to improve the mechanical performance of the obtained PBG up to a concentration of about 65 wt.% [8,9]. This was related to the attained nominal Al/P molar ratio, considered optimal when close to 1, as commonly observed in aluminophosphate minerals and zeolites [10].

A similar behavior has been extensively discussed for geopolymers obtained by reaction of MK with an Na,K-silicate solution, which harden through analogue dissolution-polycondensation reaction steps controlled by the alkali/Al molar ratio [1]. The presence of a crystalline product ($AlPO_4$) and of an amorphous network exhibiting Si–O–P–O connectivity were proposed on the basis of results of X-ray diffraction and infrared spectroscopy, respectively [8]. More recent results pointed instead to Al–O–P and Si–O–Al distinct amorphous products[11]. In addition, due to the

low solubility of silica in the acidic environment, during MK incongruent dissolution the Si-rich amorphous domains of high specific surface area are left behind [12,13]. It follows that the final product exhibits intrinsic heterogeneity on a length scale of a few hundred nanometers. Depending on the liquid-to-solid weight ratio (L/S) and H_3PO_4 concentration of the solution, the viscosity of the reactive mixtures of PBG may also be very high (up to 7 MPa·s in concentrated systems)[9]. It is of interest to gain control over the rheological properties in view of considering the material for specific applications, such as for 3D printing or sprayable coatings [14,15]. The viscosity of the as-prepared ('fresh') reactive mixture was found to decrease with the increase in water content at the same nominal Al/P, as well as with the increase in the Al/P maintaining the same L/S [16]. These changes were associated to structural modifications in the amorphous networks whose nature could not be fully ascertained. Moreover, they also impacted on the apparent rection kinetics, detected as time to set (e.g., to form the monolith). So far, there is no information on the time-evolution of the bulk rheology during the PBG setting reaction, as well as on the time-evolution of the microstructure. Because they are closely linked to the reaction mechanisms, their investigation may help to shed light on the reaction mechanisms in PBG. One of the main difficulties encountered in previous studies was to tackle the gelation/densification steps. In fact, they are non-equilibrium processes and, as such, are difficult to describe experimentally because they exhibit relevant structural and dynamical changes that span a wide range of time and length scales.

Among the few methods that allow the tracking of the microstructure and dynamics of disordered materials at the nanometric scale is the scattering with coherent light. In this respect, X-ray photon correlation spectroscopy (XPCS) has been successfully applied to investigate a number of systems in soft and hard-condensed matter science [17,18]. In this work, XPCS was employed to follow the changes in structure and dynamics during the formation of two distinct PBG formulations, differing in the concentration and amount of acid phosphate solution, with a direct impact on the overall kinetics and paste rheology. Compared to bulk rheology and dielectric spectroscopy, rarely documented for these systems [16,19], XPCS is well-suited to obtain information on the rheological and dynamical response of PBGs. In fact, bulk rheology suffers from a limited capability of elucidating heterogeneities, which play a crucial role in determining material performance, whereas addressing dynamic issues allowed us to gain insights into the physics behind the processes.

II. Materials and Methods

A. Sample preparation

The PBG samples used in this study were prepared by mechanically mixing a phosphoric acid solution with industrial metakaolin (Mephisto L05) obtained from České lupkové závody, a.s. (Czech Republic) and produced by kaolinite de-hydroxylation at high temperature (750 °C for 2h). Two different formulations, which, according to the literature [20,21], promote MK dissolution and reactivity, were prepared: the first one attaining an Al/P molar ratio of 1.5 and a L/S of 0.9, adopting a phosphoric acid solution 60 wt.% and a second one with Al/P molar ratio 1, L/S=1.2, adopting a phosphoric acid solution 63 wt.%.

At room temperature, the poly-condensation step, leading to the solidification of the material, is extremely slow and may take several days; for this reason, it is found convenient to accelerate the consolidation by heat treatment at 40 – 70 °C for few hours. In our case, the temperature of 60 °C has been adopted.

For the *in-situ* rheological tests, after mixing, the obtained slurry was transferred to the rheometer cup and equilibrated at 25 °C before starting the test procedure detailed below.

For the XPCS experiment, after mixing, the obtained slurry was injected in 2 mm ∅ glass capillaries by means of a syringe. The capillaries were sealed at one end and placed vertically on the sample stage for data collection at room temperature. Aging was obtained by placing the prepared sample capillaries in oven. The first measurement was conducted on the two formulations immediately after preparation (time 0). Then, the capillaries were kept at 60 °C and extracted at different times (1h, 3h, 6h, 16h) for data collection. For the *ex-situ* tests, it is assumed that out of the oven, at room temperature, the sample ageing is virtually 'quenched', and the reaction is restarted once back in the oven [11].

The naming convention used throughout this article will be X_Y_Z, where X identifies the L/S (09 for 0.9 and 12 for 1.2); Y identifies the concentration of phosphoric acid (60 for 60 wt.% and 63 for 63 wt.%); Z identifies the aging time (in hours).

B. Analytical Methods

Rheological measurements were performed with a Brookfield rheometer DVNXRV (Brookfield, USA) mounting an RV7 spindle. The relaxation of the residual stresses before each measurement was obtained by a pre-shear cycle to ensure the same starting conditions for all tests.

Measurements were performed *in-situ* after equilibration at 60 °C in shear stress-shear strain

mode and dynamic viscosity (η) was obtained by averaging data collected for 1 min at a speed of 50 rpm in the linear regime. The adopted experimental protocol entailing shear-rate-growth and shear-rate-descending was similar to the one reported in other works on acid-base cements [22,23]. For a second set of samples, the measurements were conducted *ex-situ*, that is, after equilibration at 25 °C with aging obtained by placing the samples in oven at 60 °C for different times. Additional dynamic rheological measurements were performed using a stress-controlled rheometer MCR Evolution Series (Anton Paar) in parallel plate geometry. After the preparatory step, a series of strain sweep tests of increasing amplitude, aimed at assessing the critical strain marking the end of the linear regime and ensuring the reproducibility of the measurements, were conducted at T = 25°C and angular frequency 10 rad s^{-1}.

The complex shear modulus $G^* = G' + iG''$ was measured bringing the samples at 60 °C *in-situ* and by applying strain oscillations of amplitudes lower than the critical strain of the network, that is, 0.05% for the sample 09_60 and 0.01% for the sample 12_63 at angular frequency 6.2832 rad s^{-1}. Measurements were stopped after 1h and 3h for sample 09_60 and 12_63, respectively, to prevent deformation of the test geometry.

XPCS data have been collected in small-angle X-ray scattering (SAXS) geometry at the beamline ID10 of the European Synchrotron Radiation Facility (ESRF), Grenoble, France covering a range in q from 0.07 nm^{-1} to 2.6 nm^{-1} [24]. A 21.67 keV beam was monochromatized with a Si(111) crystal, and its partially coherent part was selected by means of a set of slits and focused to a 16 μm × 65 μm spot at the sample position, resulting in a flux of 4.0 10^{11} photons/s. Guard slits were positioned a few cm upstream of the sample to remove the parasitic scattering produced by the primary slits. Forward scattering patterns were recorded on a EIGER 4M (2,070 × 2,167 pixels, 75 μm pixel size) placed 5.0 m downstream of the sample. A fast shutter placed upstream of the sample was synchronized with the detector to avoid unnecessary sample irradiation. The negligible time-evolution of the sample dynamics at room temperature (i.e., once removed from the oven) allowed the collection of thousands of frames with exposure times in the range of 0.05 ÷ 1 s.

III. Results and discussion

A. Rheology

The recorded rheological response at 25 °C, as viscosity vs. shear rate and shear stress vs. shear rate (plots are provided as supplementary material Fig. S1) evidenced a shear thinning behavior for the PBG samples. Similar behavior has been also observed in fresh geopolymers obtained by MK dissolution in alkaline environment [25,26]. The values of viscosity η resulted higher in 09_60 respect to 12_63, as also confirmed by the fresh reactive mixtures measured during *in-situ* aging (Fig. 1): 19.1 Pa·s for 09_60 and 6.8 Pa·s for 12_63. Notably, the time-evolution of η in the former sample follows a steeper increasing trend, such that the value after 1h is very close to the value reached after 3h in 12_63. The *ex-situ* viscosity tests produced very similar results (see supplementary material Table I), indicating that in this way the aging process was effectively 'quenched' [11], thus, the XPCS results can be considered equivalent to those of an *in-situ* experiment.

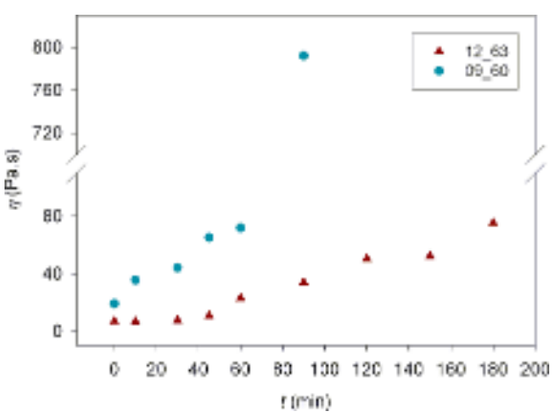

Fig. 1. Time-evolution of the viscosity of PBG samples during aging at 60 °C.

Previous results indicated that dilution of the liquid component (by increasing water content) reduced η [16] of the pastes, which may explain the lower value exhibited by the sample 12_63 at time t = 0, when there is virtually no Al in solution [27]. The slower time-evolution of this sample should be ascribed to the slower kinetics, since there is agreement in the literature regarding the accelerating effect of the nominal value of Al/P on the apparent overall reaction rates [16].
Insights into the mechanisms at the origin of the rheological behavior may be gained from the dynamic tests. Fig. 2(a) illustrates results of some of the strain sweep measurements conducted at

25 °C on the two formulations, which allowed to identify the amplitude of the strain oscillations in the linear viscoelastic regime adopted in the time-resolved tests. At low applied strain, the linear regime is characterized by a flat response of the moduli; the energy supplied is reversibly stored in deformations and the material behaves as solid. *G*' is higher than the loss modulus *G*" until a critical value of strain, beyond which *G*' decreases and the material starts to flow. *G*' and *G*" curves eventually cross at higher stress, and the viscous character dominates. In principle, the yield stress (σ_0) can be estimated from the results of strain sweep measurements [28,29]. The yield stress can be defined as the point when the structural breakdown in the material allows the viscous flow to initiate. Despite this clear definition, there is no univocal approach to its experimental determination [29–31]. To date, results from PBGs are few [32], therefore our results will be also compared with MK-based alkaline geopolymer pastes and acid-base cements, characterized by dissolution-polycondensation reaction paths. All in all, literature data on σ_0 were obtained adopting different experimental methodologies [25,26,32–38]; for our purposes, we follow the definition that identifies σ_0 as the crossing point of *G*' and *G*" according to [33]:

$$\sigma_0 = G^* \cdot \gamma_{G'=G"} = \left(G'^2 + G"^2\right)^{0.5} \cdot \gamma_{G'=G"} \quad (1)$$

The $\gamma_{G'=G''}$ was located between 0.5 and 2%; the obtained σ_0 ranged between 23–27 Pa for 12_63 and 105–130 Pa for 09_60. The former sample exhibits values comparable to those reported for some fresh alkaline geopolymer pastes [25,26,33,34], whereas higher values, around 100 Pa and above (i.e., similar to 09_60), have been reported for some PBGs formulations and acid base-cements [35–38].

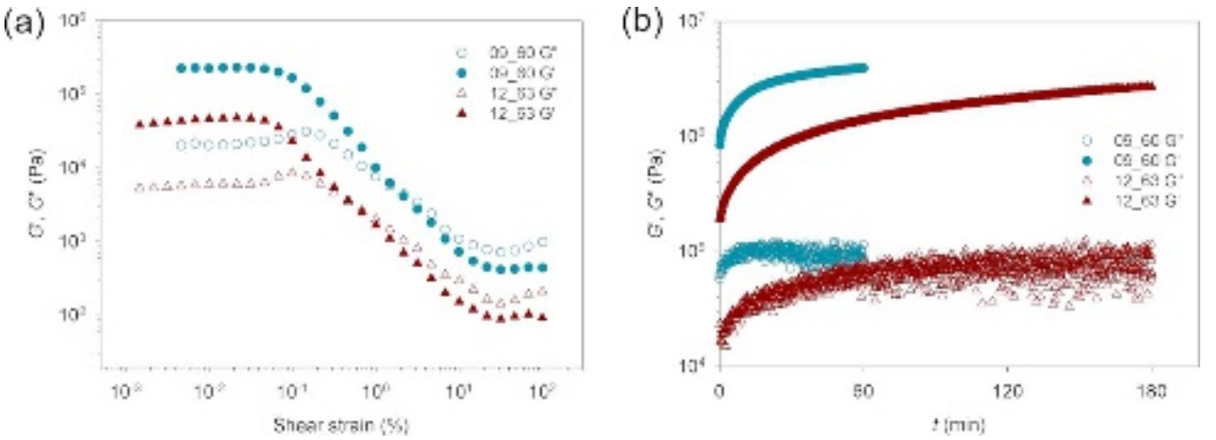

Fig. 2. Examples of results of strain sweep tests for the indicated samples at (T = 25 °C) and ω= 6.2832 rad s^{-1} (left); evolution of viscoelastic parameters during ageing at 60 °C at 6.2832 rad s^{-1} (right).

The mechanisms of energy storage in the PBGs samples have been studied in fresh MK-based alkaline geopolymer pastes [26,27,33]. In these works, the critical strain marking the end of the linear regime was observed at about 0.1% [27,33], similarly to our samples (Fig. 2(a)). It was shown that, in these formulations, because of the low volume fraction of solid added to the solution, the colloidal interactions between the grains of MK are negligible, whereas the viscosity is controlled by the development of an Al—rich gel forming very early at or near the surface of the MK grains. The early formation of this percolating network with surface fractal dimensions, was found consistent with the time-evolution of the viscoelastic moduli [39]. Notably, the viscoelastic parameters exhibited a time evolution similar to the one recorded in the samples of PBG investigated here (Fig. 2(b)) [27,33,39,40]. The curves are characterized by an initial fast increase followed by a slower pseudo-linear increase of the modulus. It is reasonable to suppose that the values of the moduli recorded in our tests differ from those formed in alkaline geopolymers because of the different type of gel formed. We also note that in the PBG samples it is likely that the very beginning of the curves illustrated in Fig. 2 was not captured by the experiment due to the time needed to equilibrate the samples at the measuring temperature of 60 °C. Nonetheless, it is evident that both formulations are dominated by the elastic modulus (as observed in the strain sweep tests in the linear regime at 25 °C). According to the model described above, the yield stress is controlled by the percolation of the gel between the MK particles. The gradual increase in the elastic modulus should be ascribed to the progressive thickening of this gel, which has

been linked to the kinetics of dissolution and diffusion of Al [27] and thus depends on solution composition. This explains both the faster time-evolution and the higher values exhibited by sample 09_63 (Fig. 1-2). In addition, the process produces an inhomogeneous distribution of Al in solution and, consequently, of the precipitated gel. The solution was found to possess a nearly pure viscous behavior, which evolves as the composition evolved during the progress of the reaction.

The abrupt change in slope after 1h illustrated in Fig. 1 by the sample 09_60 marks the formation of the monolith by the stiffening of the gel network, which is conventionally referred to as the material setting [27]. Setting is producing a similar abrupt increase in modulus, as documented in alkaline geopolymers [27]. The event was not captured in Fig. 2 because the measurements were stopped in order to preserve the instrument integrity.

B. Evolution of the microstructure

The $I(q)$ SAXS curves resulting from the azimuthal average of the SAXS intensity recorded by the detector are illustrated in Fig. 3 in a double logarithmic plot. The 09_60_16 was lost because the capillary broke inside the oven, perhaps due to material expansion. Common to all the spectra is the presence of a scattering regime at low q (< 0.3 nm^{-1}) in which the intensity scales with q^{-n}, with $n = 3.2 \div 3.4$, and of an interference peak at about 0.6 nm^{-1}. Similar features have been reported during the formation of acid-base cements based on magnesium oxide and potassium phosphate (MPCs) [41]. In the time interval covered during the experiment, a progressive decrease in scattering intensity is observed at low q, whereas at high q (> 1 nm^{-1}) the scattered intensity decreases up to 3h to increase later, with sample 12_63 exhibiting a more marked time-evolution.

Although the SAXS profile contains information on the shape and size distribution of the scattering centers, the interpretation of the signal on a sound physical basis may be challenging and is model-dependent. However, the analysis of the slope of the scattering curves provides information about the nature of the scattering surface. This approach has been adopted for geopolymers and acid-base cements, exhibiting similar dissolution and densification steps [40,42–45]. The exponent in the low q region is diagnostic of scattering from surface fractals with fractal dimension $D_S = 6–n = 2.6 \div 2.8$, covering a range of length scales (defined as $2\pi/q$) from 21 to 91 nm. In analogy with the above-mentioned systems, this scattering region includes a

contribution from the incompletely dissolved grains of MK. Conversely, the products of the PBG polycondensation reaction should give a negligible contribution to the scattering in this *q*-range; in MK-based alkaline geopolymers, the products of MK dissolution and reaggregation into small units of the gel have been reported to contribute to the $I(q)$ mostly at higher q (> 0.5 nm^{-1}) [40,45]. Therefore, the small increase in intensity detected above ~1 nm^{-1} can be ascribed to this process.

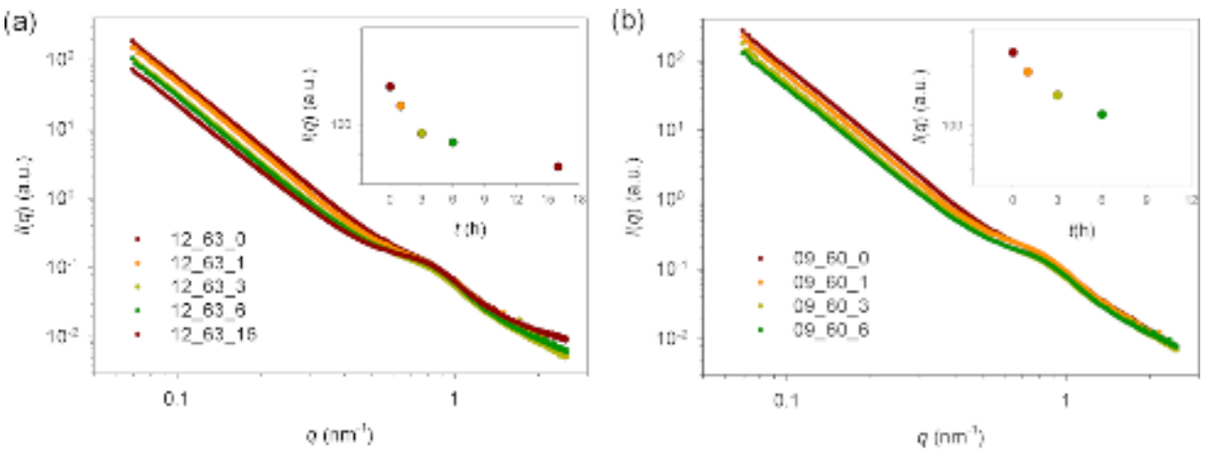

Fig. 3. SAXS curves of samples at different times, as indicated. Insets illustrates the time-evolution of the $I(q)$ for q = 0.072 nm^{-1} using the same scale for $I(q)$.

As for the fractal dimension and the $I(q)$ trend at low q, a similar surface fractal structure with D_S = 2.7 was reported to form in the first reaction stages of MPCs, reflecting the accumulation of the reaction products at the grain surface [41], a process bearing analogies with the early formation of the C–S–H gel in Portland cement [46], and consistent with the mechanisms of development of the macroscopic elastic modulus described above. In fact, at the beginning of the reaction the system is diluted and the low q region may be thought to represent the structure of the large-scale aggregates of the gel around the dissolving MK grains and possessing surface fractal scaling. It can be argued that, with time, a contribution from the growing solid matrix-pore interface increases, and, as a consequence, this densification process is accompanied by a coarsening of the microstructure, which produces a decrease in the scattering intensity at low q, in analogy with the abovementioned systems and the densification processes in nanophase ceramics in the same q-range [47–49].

C. Evolution of the dynamics

The two-time correlation function is calculated for each defined value of q as:

$$G(t_1, t_2, q) = \frac{\langle I_p(q,t_1) I_p(q,t_2)\rangle_p}{\langle I_p(q,t_1)\rangle_p \langle I_p(q,t_2)\rangle_p} \quad (2)$$

where $I_p(q, t)$ is the pixel intensity at the detector at different times t_1 and $t_2=t_1+t$, and the brackets indicate the average at the same value of q [50]. An example of two-time correlation function for the fresh sample 12_63_0, is illustrated in Fig. 4. The contours drawn parallel to the diagonal with $t_1=t_2$ are similar, indicating the negligible evolution of the dynamics due to the natural aging effect, and confirming that the time-average over ~ 15 min is, in this case, possible without loss of information.

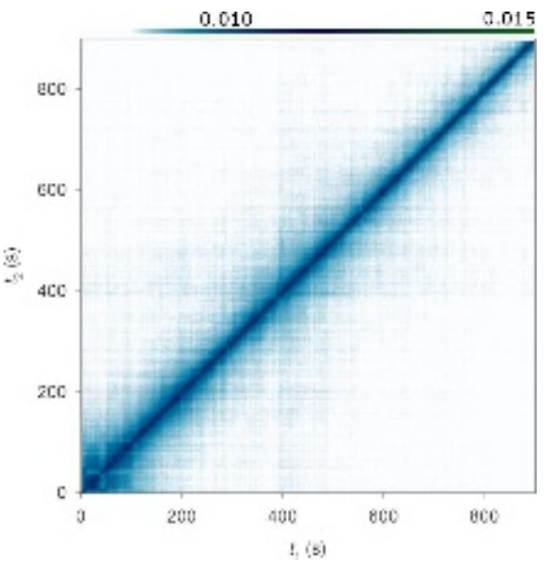

Fig. 4. Two-time correlation function observed for sample 12_63_0 and q=0.26 nm^{-1}.

Further insights into the dynamical processes can be obtained by calculating the autocorrelation function $g^{(2)}(q, t)$:

$$g^{(2)}(q,t) = \langle C(t_1, t_1 + t, q\rangle_{t1} \quad (3)$$

The $g^{(2)}$ is related to the intermediate scattering function $f(q, t)$ via the Siegert relation [51], which provides information on the density fluctuations within the material, and is typically fitted to the Kohlrausch-Williams-Watts (KWW) exponential function:

$$g^{(2)}(\tau) = 1 + \beta_i |f(q,t)|^2 = 1 + \beta_{exp} \exp\left[-2\left(t/\tau(q)\right)^{\gamma(q)}\right] \quad (4)$$

where β_i is the instrument contrast, which was determined using a static vycor sample, t is the lag time, $\tau(q)$is the apparent relaxation time, and $\gamma(q)$ is the stretching exponent or shape parameter, which, together with the dependence of τ on q, is related to the kind of observed dynamics. For Brownian motions, $\tau \propto q^{-2}$ and $\gamma = 1$, for ballistic dynamics, $\tau \propto q^{-1}$ and $\gamma = 2$ [52], while many arrested systems exhibit some intermediate behavior of γ with τ scaling as q^{-1} [53–57].

The analysis of the autocorrelation functions determined along the vertical (here, azimuthal angle $\phi = 0° \pm \Delta\phi$) and horizontal ($\phi = 90° \pm \Delta\phi$) directions showed a marked anisotropy. Fig. 5(a) illustrates these different regimes for two values of q in the sample 12_63_0, with a faster decay in the vertical direction. The samples 12_63 exhibited a two-step decay of the intermediate scattering function, with the exception of 12_63_1 and 12_63_16, where the slowest relaxation was outside the time window set by the duration of their respective XPCS measurements. The two-step decay is frequently modeled with empirical functions, such as the linear sum of two stretched exponentials[58,59]:

$$f(q,t) = b \exp\left[-\left(t/\tau_1(q)\right)^{\gamma_1(q)}\right] + (1-b) \exp\left[-\left(t/\tau_2(q)\right)^{\gamma_2(q)}\right] \quad (5)$$

This type of relaxation behavior is documented for a wide range of disordered structures, including glasses, colloidal gels, emulsions and foams. The fast decay is commonly ascribed to the motions of individual particles or small clusters confined in the cage formed by their neighbors, whereas the slow relaxation may display different dynamical features (e.g., diffusive, subdiffusive, ballistic, hyperdiffusive) and it is thought to reflect structural rearrangements of the bond network at larger length scales [58–61]: It should be observed that in systems going towards structural arrest, the slower decay is typically characterized by temporal and spatial heterogeneities, where the former produces temporal fluctuations of the dynamics, and the latter

is responsible for changes at different position on the sample [60,62]. This may probably explain its absence from 12_63_1 and 12_63_16.

In order to link the time-evolution of the macroscopic rheology, the microscopic dynamics and the underlying reaction mechanisms, our analysis will be mainly focused on the study of the fast component, common to both studied samples, by fitting the autocorrelation functions using Eq. (5) for samples 12_63, whereas for sample 09_60 the fit has been conducted adopting Eq. (4) (examples of fits are reported in Fig. 5 and in the supplementary material Fig. S2), whereas example of fit showing the two relaxation components, as obtained adopting Eq. (5) is reported as supplementary material Fig. S3.

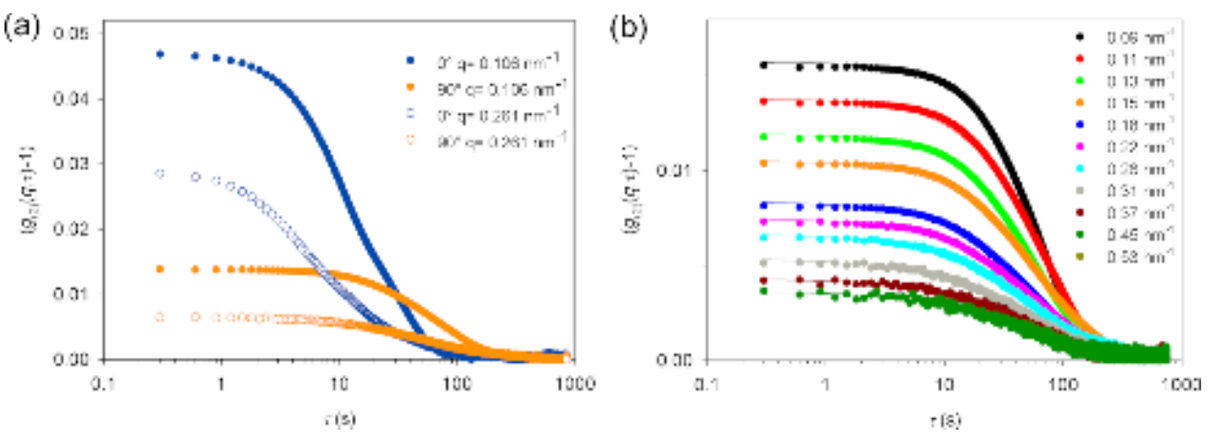

Fig. 5. (a) Intensity autocorrelation functions in the vertical (ϕ = 0°) and horizontal direction (ϕ = 90°) for two values of q, as indicated, in the sample 12_63_0; (b) set of intensity autocorrelation functions of sample 12_63_0 for the indicated values of q at ϕ = 90°. Solid lines are fits to Eq. (4).

The q-dependency of the relaxation rates ($1/\tau$) in the horizontal direction for the investigated samples at different aging times is illustrated in Fig. 6, and supplementary material Fig. S4 for the slow relaxation process. The results of the fit evidenced for both the relaxation processes and samples a q^{-1} scaling, which is accompanied by a faster-than-exponential decay of the correlation function, with the stretching exponent γ around 1.5 and decreasing with q. Notably, both 'fresh' samples (aging time = 0) behaved differently, exhibiting a q^0 scaling and $\gamma > 1$.

The q^{-1} regime and the compressed shape of the autocorrelation function with $\gamma \sim 1.5$ has been documented for a number of arrested systems, such as colloidal gels, polymer nanocomposite

melts, polymer aerogels, and other soft matter disordered systems [53–57,63]. According to previous models, such faster than diffusive motion has been interpreted as the result of the relaxation of residual stress dipoles randomly distributed inside the sample [57,64]. There is indication that such systems are also characterized by a marked heterogeneity of the dynamics.

As for the *q*-independent modes, they were found to be a feature common to many complex systems with slow dynamics when the probed length scale is much larger than any nearest-neighbor distance in the system [65–67]. Their origin has been associated with the presence of independently relaxing regions in absence of single-particle diffusion and suggests the presence of a crossover to diffusive dynamics ($\tau \propto q^{-2}$) at even smaller q [67,68]. In fact, this type of relaxation dynamics has been observed adopting light scattering in some semi-diluted polymers and rodlike micelles, as well as in DNA-based transient networks [68,69]. The presence of finite τ in a range of q has been observed also in liquid systems with other X-ray based techniques [70,71], whereas, in XPCS experiments, it has been reported for fluidized glasses, associated with stretched relaxation [72,73].The situation presented here, however, is slightly different, since $\tau \propto q^0$ is accompanied with a compressed relaxation, which makes a straightforward association to an existing theoretical framework difficult.

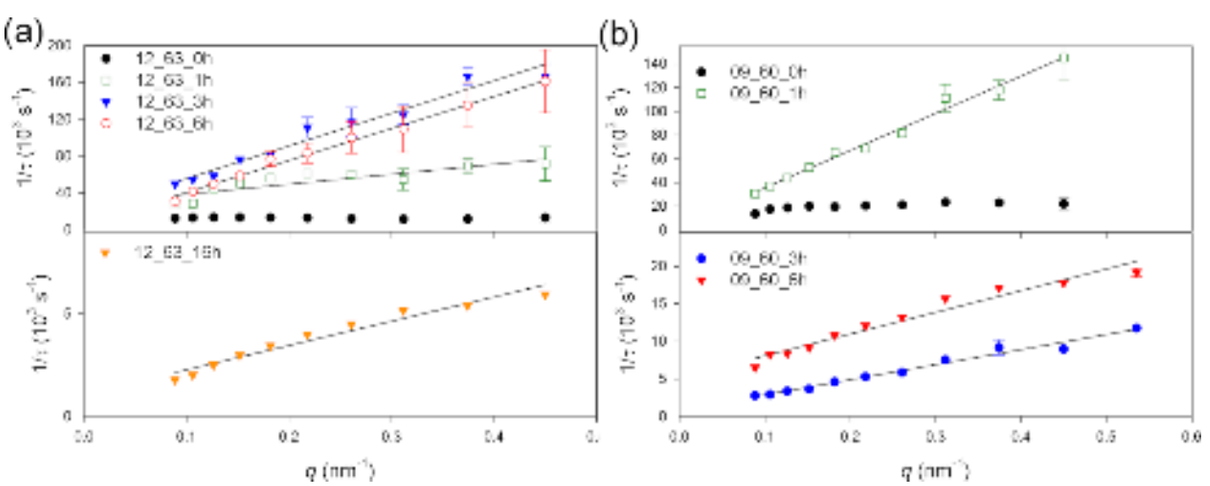

Fig. 6. Relaxation rate (1/ τ) vs. q in the horizontal direction for the two samples at different times, as indicated. Solid lines represent the linear fit through the data. Standard errors within symbols are omitted.

The marked difference in the relaxation dynamics along the horizontal and vertical directions indicates the presence of anisotropic stress fields, which are attributed to the different boundary conditions experienced by the material within the capillary in the two directions (e.g., due to adhesion to the capillary walls), rather than being an effect of sedimentation [74]. In fact, sedimentation should give rise to oscillations in the autocorrelation function in the vertical direction, which are not observed here [75]. Moreover, at variance with sedimentation experiments, from 1h onward, no deviations from the q^{-1} regime occurred [75].

As illustrated in Fig. 7, the asymmetry in the stress relaxation vanishes at long ages in both samples, whereas the relaxation rates are low in the fresh samples, exhibit a maximum between 1 and 3h, and decrease thereafter. Moreover, irrespective of the azimuthal direction, the maxima in the $1/\tau$ vs. time plots are shifted at longer times in the sample 12_63, pointing to a slower time-evolution of the aging process. The slow relaxation (plots are provided as supplementary material Fig. S5), seems to replicate the same trends, although with less points.

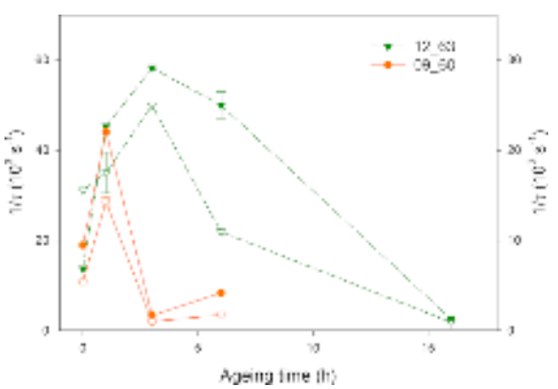

Fig. 7. Relaxation rate vs. aging time for both samples in the horizontal (full symbols, left axis) and vertical (empty symbols, right axis) direction and q = 0.126 nm^{-1}. Standard errors within symbols are omitted.

The plateau at small lag times of the intensity autocorrelation functions, defining the experimental contrast b_{exp} (Fig. 5(a)), also shows a remarkable time-evolution, that is, at time 0, the values are significantly lower in the horizontal direction with respect to the vertical direction, but this difference is sensibly reduced already after 1h and is vanishing afterwards.

Values of b_{exp} lower than the Siegert factor b_0 are a telltale indicating the presence of processes faster than the time-window probed by the experiment. The analysis of the dependence of b_{exp} on q and time provides information on the fast motions outside the experimental time-window. The accepted model for glass-like materials assumes semi-localized motions, with particles constrained by their neighbors and with the intermediate scattering function decreasing with q to the non-ergodicity factor f_q [55,74,76,77], expressed in the form of the Debye-Waller factor:

$$f_q = f_0 \exp(-q^2 r_{loc}^2/6) = b_{exp}/b_0 \quad (6)$$

where r_{loc} is the localization length, which characterizes the range of fast, localized, motions in the system; f_0 is the fraction of particles in the scattering volume exhibiting localized motions with average root-mean-squared displacement r_{loc}, whereas $1-f_0$ is the fraction of scatterers free to move over a range of lengths >> $1/q_{min} \approx 11.3$ nm.

According to Eq. (6), r_{loc} and f_0 were calculated by fitting the negative logarithm of b_{exp}/b_0 as a function of q^2 (Fig.8). Points at low q are likely influenced by the structure factor [76,78], which, in our case, could not be reliably determined. Thus, the first three points, which deviated from the linear behavior, were excluded. Fig. 8(b) shows that in both PBG samples $f_0 < 1$ at time 0, confirming the presence of a fraction of fast-moving particles. After 1h, this population almost completely disappeared, and at 3h, all the dynamics are localized ($f_0 = 1$). Along with the vanishing fraction of particles exhibiting non-localized dynamics, r_{loc} decreases over time, indicating increasingly restricted motions, interpreted as the stiffening of the network leading to the formation of the monolithic structure [74,76,77].

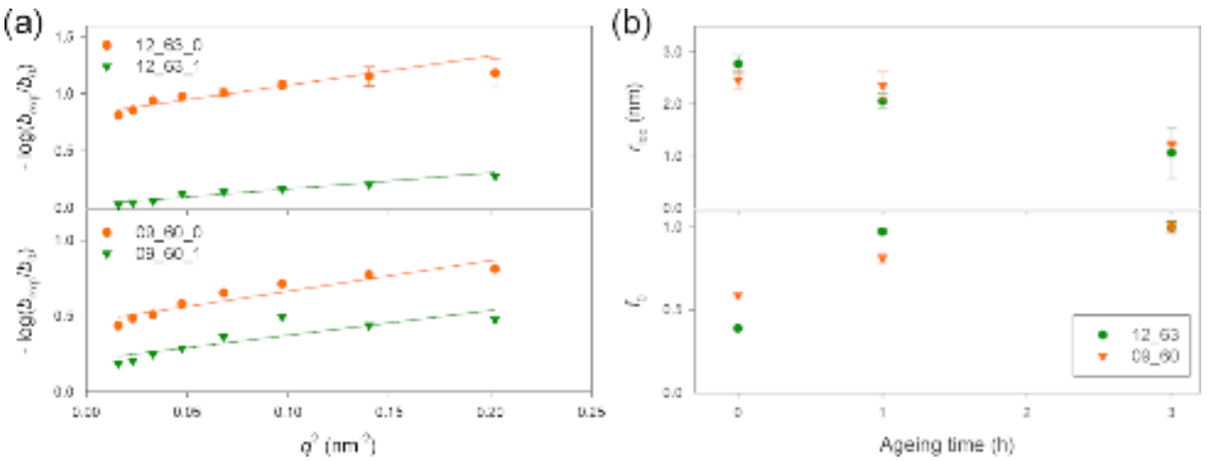

Fig. 8. Negative logarithm of the non-ergodicity factor b_{exp}/b_0 vs. q^2 at time 0 and 1h, as indicated (a) in the horizontal direction. Solid lines are fit to the Eq. (6). Localization length r_{loc} ((b) top) and fraction of particles exhibiting localized motions f_0 ((b) bottom) up to 3h. Standard errors within symbols are omitted.

D. A unified model for the PBG reaction

Bulk rheology and the analysis of the non-ergodicity factor indicated monotonic trends, although with different characteristic times, for the two reacting PGB samples. This apparently conflicts with the 'peaked' time-evolution of the relaxation rates depicted in Fig. 7. However, when considering the origin of the missing contrast, the results may be consistent with a scenario in which the fraction of particles with fast dynamics progressively enters the experimental time-window as the system evolves towards structural arrest, thus producing the apparent increase in the relaxation rates observed between 1 and 3h; eventually, at longer times, the overall slowdown of the dynamics prevails, and the relaxation rates drop.

Similar dynamic heterogeneities, encompassing populations of particles exhibiting localized and delocalized motions, have been observed in many systems approaching structural arrest [79–81]. In gel networks, dynamic heterogeneity appears to be linked to large scale structural heterogeneity for a wide range of densities; such inherently structurally heterogeneous nature of the formed networks has been confirmed by numerical simulations and experimental works [82,83].

As previously mentioned, intrinsic heterogeneity has also been confirmed for the aluminosilicate gel formed from MK dissolution in alkaline environments, which exhibits a time-evolution of

rheological properties analogous to PBGs [27]. Some amorphous materials in the system SiO_2–Al_2O_3–P_2O_5 were found to consist of domains rich in $AlPO_4$ and SiO_2 structural units [84,85]. PBGs possess analogous structural heterogeneity at the length scale of the order of hundreds of nm [21], owing to the coexistence of a network with Al–O–P bonds and a hydrated silica network formed by the rearrangement and amorphization of the residue of MK dissolution [86]. To date, information regarding their structural details is incomplete. Dissolution experiments of MK in sulfuric and hydrochloric acid evidenced the formation of a mesoporous amorphous silica material with pore size distribution peaked at 1.7÷3 nm [86–88]. An aerogel prepared to replicate a silicate glass hydrated alteration layer at pH = 3 exhibited an open porosity mostly between 6 and 9 nm, although the porosity and the size of the scattering objects derived from the SAXS curves were found to depend on the reaction conditions [89]. However, in analogy with our PBGs (Fig. 3), the $I(q)$ evidenced a broad interference peak spanning the range 0.4 ÷ 1 nm^{-1}, ascribed to the scattered intensity from small dimers or trimers with radius of gyration ~ 3 nm incorporated into larger structures contributing to the main slope. This was found in agreement with the formation of silica gel networks by the coalescence of clusters that, owing to the silica low solubility and surface charge at low pH, are aggregates of randomly branched chains [90].

In order to obtain additional structural information on the PBG reaction products, an empirical model developed for gels [91] and adopted to describe the nucleation of the phosphate hydrate amorphous products in MPC [41], was applied. The $I(q)$ was fitted to a linear combination of a power law, which accounts for the scattering at low q, a broad peak function, and a flat background. The intensity was calculated as:

$$I(q) = \frac{A}{q^n} + \frac{C}{1+(|q-q_0|\,\xi)^m} + B \qquad (7)$$

where A is the power law scale factor, n is the power law exponent, C is the scale factor of the peak function, ξ (which is the inverse of the peak half-width-at-half-maximum) is the correlation length, q_0 is the peak position, and B is the incoherent flat background. The exponent m refined to values close to 2, defining a Lorentzian shape. The increase in $I(q)$ at high q for 12_63 was not modeled, given the too short q range available. Numerical results and a graphical example of the least squares fit are provided in the supplementary material.

The first term, the low q feature, characterizes the fractal structure of large clusters, whereas the peak position describes the average distance between large structures (d = 8.6÷10.3 nm) [41,92–94]. The correlation length ξ (2.5÷3.5 nm), characterizes the internal structure, similar to the mesh size in gel networks [92,95,96], and is ascribed to the density fluctuations originating from smaller clusters. A comparison with the results reported for MPCs (d ~ 7.9 nm and ξ ~ 3 nm), suggests some structural similarities with PBG, likely related to their common dissolution-condensation mechanisms.

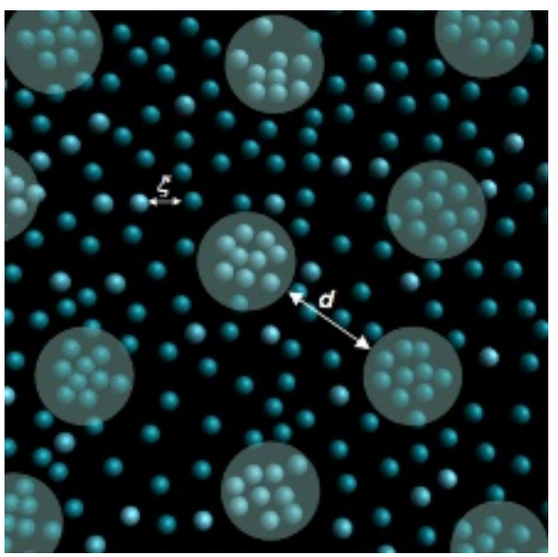

Fig. 9. Representation of the PBG network with phase-separated regions (indicated by the circles) separated by a characteristic length scale, d and characterized by mesh size ξ.

In MPCs, the amorphous phosphate networks were thought to form very early, owing to the high dissolution rates of the oxide, by the coalescence of clusters of PO_4^{3-} and solvated magnesium units [97,98]. The system ages through a 'densification' process entailing a decrease in SAXS intensity at low q, a decrease in the fraction of mobile scatterers, a decrease in their diffusing volume, and a decrease in the number of mesopores [41]. In fact, such trends are replicated by the PBG samples, as illustrated in Fig. 2 and Fig. 8(b).

It can be conjectured that in PBGs, the networks also start to form very early in the freshly prepared samples, with the dissolution of MK and the accumulation of products near and at the surface of MK, owing to the high concentration gradients [13]. This explains the occurrence of the surface fractal scaling with D_S ~ 2.7, already observed in MPCs, as well as in alkaline

geopolymers and synthetic aluminosilicate networks [39,43]. In fact, similar values are typical of highly concentrated systems, when the density allows for the formation of percolating networks, irrespective of the cluster aggregation mechanisms (otherwise predicting a lower fractal dimension) [99]. This also agrees with the time-evolution of the viscoelastic moduli (Fig. 2), which we have proposed to originate owing to the early formation of a percolating network with surface fractal dimensions. The low pH attained favors the formation of small Si polymeric units, which interpenetrate each other (entangle), forming additional branches. Concomitantly, components of the aluminophosphate hydrogel network grow by gathering together in solution Al^{3+} ions released from the MK and PO_4^{3-} ions [11]. They are thought to form clusters, in analogy with the formation of the amorphous phosphate hydrate in MPCs. In the freshly prepared samples, at the initial stages of the densification process, these building blocks are already arranged in large structures and only a small fraction of scattering objects is allowed to freely diffuse, as indicated by the fraction of particles exhibiting fast dynamics detected with XPCS (Fig. 8(b)). With aging, the dynamics become localized, as their movement is restricted by the growth and stiffening of the finely intermixed networks. The localized motions are confined to a volume that coincides with the size of the mesh network defined by the SAXS model. Moreover, the small but clear decrease in both d and ξ with aging, points to a densification process, as observed in gel networks [95]. In reason of the higher amount of potentially available Al, favoring the formation of the hydrated silicate and aluminophosphate networks, the process is faster in 09_60, as confirmed by their time-evolution, the time-evolution of the dynamics (Fig. 7), of the fraction of freely diffusing particles (Fig. 8(b)), and the mechanical response (Fig. 1-2).

This view bears similarities with the description of amorphous domains of alkaline geopolymers, colloidal gels and glasses as percolating networks, in which confined motions occur within the network, whereas the mobile particles are located in the voids and in proximity to the network surface [39,76,100–102]. However, unlike alkaline geopolymers, in which the formation of a rigid network is connected with the segregation of water, in PBGs (and MPCs), the water is progressively subtracted and incorporated into the products, progressively hindering the ion and particle mobility [97].

We speculate that the basic network topologies in the freshly prepared samples are already present at the time of the XPCS measurements. The q-independent relaxation mode characterizing the collective density-density correlation function (Fig. 6) has been proposed to

stem from the density fluctuations of the molecular network undergoing reconfiguration without significant mass transport [67]. This suggests that the structural evolution and the recorded densification occurred through minor rearrangements and limited long range particle diffusion. This picture is consistent with the recently proposed evolution of gel systems towards mechanical stability (aging) attained by forming a percolated structure through events of bond stretching/breaking and by increasing the overall compaction [103]. The internal stresses, which are concentrated in the weak part of the network, are released during this coarsening process, and the relaxation of such independent regions is reflected in the compressed exponential regime detected in the aging samples with XPCS. Coherently, the SAXS curves preserved their main features, comprising a contribution from the large gel structures, described by their surface fractal scaling, and a network with average mesh size ξ with inhomogeneities characterized by their distance d. The declining $I(q)$ at low q is the result of the microstructure coarsening with the development of a denser body [47] accompanying the entire aging process all the way through the formation of the monolith (Fig. 9).

IV. Conclusions

In this work we report the time-evolution of the dynamics, microstructure and mechanical response of two phosphate-based geopolymer formulations. The overall picture suggests a scenario in which the Al/P molar ratio and water content of the raw mix impact on the reaction path (entailing dissolution-condensation) through the evolution of two distinct amorphous gel reaction products.

The key findings are summarized as follows:

- The autocorrelation functions of the studied relaxation processes indicated that the establishment of density fluctuations and the development of internal stresses in the forming gel network are the main mechanisms that characterize the evolution of the sample dynamics towards structural arrest.
- The presence of fractions of particles exhibiting localized and delocalized motions points to dynamic heterogeneities, which are likely accompanied by structural heterogeneities. They explained the 'peaked' time-evolution of the relaxation rates, as fast scatterers progressively enter the experimental time windows with the overall slowdown of the dynamics as the system ages.

- The analysis of the small-angle scattering curves suggests a system that ages through a 'densification' process producing a declining intensity at low q as the gel reaction product forms near or around the MK particles, giving rise to a structure with fractal scaling.
- The correlation lengths model adopted to fit the $I(q)$, in analogy with gel structures, describes a network with an average mesh size coinciding with the size of confinement obtained from the analysis of the dynamics (2 ÷ 3 nm).
  Consistent with this analysis, the number of freely diffusing particles vanishes with time, whereas the volume of confinement decreases because of the restrictions imposed by the growth and stiffening of two finely intermixed networks: one containing Al–O–P bonds and hydrated silica; the latter being the residue of dissolution of the dehydroxylated clay.
- We believe that initially, complex percolating networks evolve by the addition of Al^{3+} ions released from the metakaolin and PO_4^{3-} ions in solution, on one side, and by increasing entanglement and branching of the Si polymeric units, favored by the low pH of the chemical environment, on the other.
  The later evolution is instead dominated by a limited reconfiguration of the network without significant mass transport, entailing the release of the accumulated internal stresses.
- Accordingly, the availability of Al accelerates the kinetics of the process, whereas dilution (by increasing the water content), has the opposite effect. The bulk rheology confirms these evidences with a time-evolution synchronous with the one exhibited by the dynamics. Moreover, the Al/P molar ratio of the mix, as somewhat an index of network forming ability, positively correlates with dynamic viscosity and negatively correlates with the water fraction.

Supplementary Material

The following supplementary material is available: rheological response at 25 °C shear stress-shear strain mode; time-evolution of viscosity as obtained from the samples equilibrated at 60 °C in the rheometer; set of intensity autocorrelation functions of sample 09_60_0; example of fit of the autocorrelation function to Eq. (5); plot of relaxation rate vs. q in the horizontal direction for the slow relaxation; relaxation rate vs. aging time for the fast and slow components for the

sample 12_63; description of the model adopted to fit the SAXS data; figure illustrating an example of fit of SAXS data according to the model; table of relevant numerical parameters of the model adopted to fit the SAXS data.

Acknowledgements

We acknowledge the European Synchrotron Radiation Facility (ESRF) for provision of synchrotron radiation facilities under proposal number MA5977 (DOI: 10.15151/ESRF-ES-1309938504). The authors wish to thank Quentin Wehrung for his help during the beamtime. The Czech Academy of Sciences, Institute of Theoretical and Applied Mechanics (RVO 68378297) is acknowledged for supporting this study.

Conflict of Interest Statement

The authors have no conflicts to disclose.

Author Contributions

Alberto Viani: formal analysis (lead) – writing (lead) – review and editing (equal) – methodology (equal). **Davide Bernasconi:** conceptualization (equal) – validation (equal) – resources (lead) – project administration (lead). **Lucie Zárybnická:** formal analysis (supporting) – resources (supporting) – review and editing (supporting). **Federico Zontone:** supervision (supporting) – review and editing (supporting) – formal analysis (equal). **Alessandro Pavese:** supervision (supporting) – funding acquisition (lead) – review and editing (equal). **Francesco Dallari:** conceptualization (equal) – formal analysis (equal) – validation (equal) – software (lead) – methodology (equal).

Data availability

Raw XPCS data were generated at ESRF, Grenoble, France (DOI: 10.15151/ESRF-ES-1309938504). All derived data supporting the findings of this study are available from the corresponding author upon reasonable request.

Bibliography

[1] Y.-S. Wang, Y. Alrefaei, and J.-G. Dai, "Silico-Aluminophosphate and Alkali-Aluminosilicate Geopolymers: A Comparative Review," Front Mater **6**, (2019).

[2] A. Katsiki, "Aluminosilicate phosphate cements – a critical review," Advances in Applied Ceramics **118**(5), 274–286 (2019).

[3] D. Bernasconi, A. Viani, P. Macova, L. Zarybnicka, C. Caviglia, E. Destefanis, S. Bordignon, R. Goberto, and A. Pavese, "MSWI fly ash incorporation into acid-based geopolymer: reactivity and performance impact," in *EGU General Assembly 2022*, (2022).

[4] A. Wilson, and J.W. Nicholson, *Acid-Base Cements* (Cambridge University Press, 1993).

[5] S. Louati, S. Baklouti, and B. Samet, "Acid based geopolymerization kinetics: Effect of clay particle size," Appl Clay Sci **132–133**, 571–578 (2016).

[6] M. Lassinantti Gualtieri, M. Romagnoli, and A.F. Gualtieri, "Preparation of phosphoric acid-based geopolymer foams using limestone as pore forming agent – Thermal properties by in situ XRPD and Rietveld refinements," J Eur Ceram Soc **35**(11), 3167–3178 (2015).

[7] M. Lassinantti Gualtieri, M. Romagnoli, S. Pollastri, and A.F. Gualtieri, "Inorganic polymers from laterite using activation with phosphoric acid and alkaline sodium silicate solution: Mechanical and microstructural properties," Cem Concr Res **67**, 259–270 (2015).

[8] H.K. Tchakouté, C.H. Rüscher, E. Kamseu, F. Andreola, and C. Leonelli, "Influence of the molar concentration of phosphoric acid solution on the properties of metakaolin-phosphate-based geopolymer cements," Appl Clay Sci **147**, 184–194 (2017).

[9] T. Dong, Y. Zhang, Y. Jiang, G. Zhao, and X. Yu, "Workability and mechanical property of metakaolin phosphate acid based geopolymer," IOP Conf Ser Earth Environ Sci **267**(2), 022002 (2019).

[10] X. Liu, N. Yan, L. Wang, C. Ma, P. Guo, P. Tian, G. Cao, and Z. Liu, "Landscape of AlPO-based structures and compositions in the database of zeolite structures," Microporous and Mesoporous Materials **280**, 105–115 (2019).

[11] V. Mathivet, J. Jouin, A. Gharzouni, I. Sobrados, H. Celerier, S. Rossignol, and M. Parlier, "Acid-based geopolymers: Understanding of the structural evolutions during consolidation and after thermal treatments," J Non Cryst Solids **512**, 90–97 (2019).

[12] D. Karbalaei Saleh, H. Abdollahi, M. Noaparast, and A. Fallah Nosratabad, "Dissolution of aluminium from metakaolin with oxalic, citric and lactic acids," Clay Miner **54**(2), 209–217 (2019).

[13] C. Belver, M.A. Bañares Muñoz, and M.A. Vicente, "Chemical Activation of a Kaolinite under Acid and Alkaline Conditions," Chemistry of Materials **14**(5), 2033–2043 (2002).

[14] Z. Zhao, M. Chen, J. Xu, L. Li, Y. Huang, L. Yang, P. Zhao, and L. Lu, "Mix design and rheological properties of magnesium potassium phosphate cement composites based on the 3D printing extrusion system," Constr Build Mater **284**, 122797 (2021).

[15] H. Feng, X. Zheng, Z. Yu, B. Chen, P. Zhu, J. Yu, and Z. Luo, "Development of sprayable ultra-high ductility magnesium phosphate cement-based composites based on the rheological properties," Constr Build Mater **377**, 131113 (2023).

[16] V. Mathivet, J. Jouin, M. Parlier, and S. Rossignol, "Control of the alumino-silico-phosphate geopolymers properties and structures by the phosphorus concentration," Mater Chem Phys **258**, 123867 (2021).

[17] A.R. Sandy, Q. Zhang, and L.B. Lurio, "Hard X-Ray Photon Correlation Spectroscopy Methods for Materials Studies," Annu Rev Mater Res **48**(1), 167–190 (2018).

[18] A. Madsen, A. Fluerasu, and B. Ruta, "Structural Dynamics of Materials Probed by X-Ray Photon Correlation Spectroscopy," in *Synchrotron Light Sources and Free-Electron Lasers*, (Springer International Publishing, Cham, 2018), pp. 1–30.

[19] H. Douiri, I. Kaddoussi, S. Baklouti, M. Arous, and Z. Fakhfakh, "Water molecular dynamics of metakaolin and phosphoric acid-based geopolymers investigated by impedance spectroscopy and DSC/TGA," J Non Cryst Solids **445–446**, 95–101 (2016).

[20] M. Zribi, and S. Baklouti, "Investigation of Phosphate based geopolymers formation mechanism," J Non Cryst Solids **562**, (2021).

[21] D. Bernasconi, A. Viani, L. Zárybnická, P. Mácová, S. Bordignon, C. Caviglia, E. Destefanis, R. Gobetto, and A. Pavese, "Phosphate-based geopolymer: Influence of municipal solid waste fly ash introduction on structure and compressive strength," Ceram Int **49**(13), 22149–22159 (2023).

[22] Z. Zhao, M. Chen, J. Xu, L. Li, Y. Huang, L. Yang, P. Zhao, and L. Lu, "Mix design and rheological properties of magnesium potassium phosphate cement composites based on the 3D printing extrusion system," Constr Build Mater **284**, 122797 (2021).

[23] D. Dong, Y. Huang, Y. Pei, X. Zhang, N. Cui, P. Zhao, P. Hou, and L. Lu, "Effect of spherical silica fume and fly ash on the rheological property, fluidity, setting time, compressive strength, water resistance and drying shrinkage of magnesium ammonium phosphate cement," Journal of Building Engineering **63**, 105484 (2023).

[24] D. Bernasconi, F. Dallari, A. Viani, and Q. Wehrung, *Dynamics of Dissolution/Polymerization in Phosphate-Based Geopolymers* (European Synchrotron Radiation Facility, 2026).

[25] C. Lu, Z. Zhang, C. Shi, N. Li, D. Jiao, and Q. Yuan, "Rheology of alkali-activated materials: A review," Cem Concr Compos **121**, 104061 (2021).

[26] A. Favier, J. Hot, G. Habert, N. Roussel, and J.B. D'Espinose De Lacaillerie, "Flow properties of MK-based geopolymer pastes. A comparative study with standard Portland cement pastes," Soft Matter **10**(8), 1134–1141 (2014).

[27] A. Favier, G. Habert, J.B. D'Espinose De Lacaillerie, and N. Roussel, "Mechanical properties and compositional heterogeneities of fresh geopolymer pastes," Cem Concr Res **48**, 9–16 (2013).

[28] F. Cyriac, P.M. Lugt, and R. Bosman, "On a New Method to Determine the Yield Stress in Lubricating Grease," Tribology Transactions **58**(6), 1021–1030 (2015).

[29] M. Dinkgreve, J. Paredes, M.M. Denn, and D. Bonn, "On different ways of measuring 'the' yield stress," J Nonnewton Fluid Mech **238**, 233–241 (2016).

[30] D. Bonn, M.M. Denn, L. Berthier, T. Divoux, and S. Manneville, "Yield stress materials in soft condensed matter," Rev Mod Phys **89**(3), 035005 (2017).

[31] H.J. Walls, S.B. Caines, A.M. Sanchez, and S.A. Khan, "Yield stress and wall slip phenomena in colloidal silica gels," J Rheol (N Y N Y) **47**(4), 847–868 (2003).

[32] Y.S. Wang, J.L. Provis, and J.G. Dai, "Role of soluble aluminum species in the activating solution for synthesis of silico-aluminophosphate geopolymers," Cem Concr Compos **93**, 186–195 (2018).

[33] A. Poulesquen, F. Frizon, and D. Lambertin, "Rheological Behavior of Alkali-Activated Metakaolin During Geopolymerization," in *Cement-Based Materials for Nuclear Waste Storage*, (Springer New York, New York, NY, 2013), pp. 225–238.

[34] M. Romagnoli, C. Leonelli, E. Kamse, and M. Lassinantti Gualtieri, "Rheology of geopolymer by DOE approach," Constr Build Mater **36**, 251–258 (2012).

[35] D. Dong, Y. Huang, Y. Pei, X. Zhang, N. Cui, P. Zhao, P. Hou, and L. Lu, "Effect of spherical silica fume and fly ash on the rheological property, fluidity, setting time, compressive strength, water resistance and drying shrinkage of magnesium ammonium phosphate cement," Journal of Building Engineering **63**, 105484 (2023).

[36] H. Feng, X. Zheng, Z. Yu, B. Chen, P. Zhu, J. Yu, and Z. Luo, "Development of sprayable ultra-high ductility magnesium phosphate cement-based composites based on the rheological properties," Constr Build Mater **377**, 131113 (2023).

[37] C. Ma, F. Wang, H. Zhou, Z. Jiang, W. Ren, and Y. Du, "Effect of early-hydration behavior on rheological properties of borax-admixed magnesium phosphate cement," Constr Build Mater **283**, 122701 (2021).

[38] C. Ma, G. Chen, Z. Jiang, H. Zhou, H. Yao, R. Zhou, and W. Ren, "Rheological properties of magnesium phosphate cement with different M/P ratios," Constr Build Mater **282**, 122657 (2021).

[39] J. Rouyer, and A. Poulesquen, "Evidence of a Fractal Percolating Network During Geopolymerization," Journal of the American Ceramic Society **98**(5), 1580–1587 (2015).

[40] P. Steins, A. Poulesquen, O. Diat, and F. Frizon, "Structural Evolution during Geopolymerization from an Early Age to Consolidated Material," Langmuir **28**(22), 8502–8510 (2012).

[41] A. Viani, P. Mácová, and M. Peréz-Estébanez, "Nucleation of amorphous precursor in magnesium phosphate cements: Clues to the reaction pathway," Mater Lett **304**, 130677 (2021).

[42] A. Viani, K. Sotiriadis, P. Šašek, and M.-S. Appavou, "Evolution of microstructure and performance in magnesium potassium phosphate ceramics: Role of sintering temperature of MgO powder," Ceram Int **42**(14), (2016).

[43] J.N. Mills, N.J. Wagner, and P. Mondal, "Relating chemical composition, structure, and rheology in alkali-activated aluminosilicate gels," Journal of the American Ceramic Society **104**(1), 572–583 (2021).

[44] D. Jozić, S. Zorica, D. Tibljaš, and S. Bernstorff, "Insitu SAXS/WAXS study of the developing process of geopolymer structures," in *Eccm15 - 15th European Conference on Composite Materials*, (Venice, 2012), pp. 1–8.

[45] V. Benavent, P. Steins, I. Sobrados, J. Sanz, D. Lambertin, F. Frizon, S. Rossignol, and A. Poulesquen, "Impact of aluminum on the structure of geopolymers from the early stages to consolidated material," Cem Concr Res **90**, 27–35 (2016).

[46] A.J. Allen, R.C. Oberthur, D. Pearson, P. Schofield, and C.R. Wilding, "Development of the fine porosity and gel structure of hydrating cement systems," Philosophical Magazine Part B **56**(3), 263–288 (1987).

[47] A.J. Allen, S. Krueger, G.G. Long, H.M. Kerch, H. Hahn, and G. Skandan, "Small-angle neutron scattering studies of ceramic nanophase materials," Nanostructured Materials **7**(1–2), 113–126 (1996).

[48] M.H. Al Rashid Megat Ahmad, A. Ibrahim, A.A. Mohamed, R. Alias, N.H. Alias, C.S. Mahmood, E.G.R. Putra, A. Ikram, and a. F. Awang Mat, "Study of temperature effect on microstructures of MCIC ceramic substrate using small angle neutron scattering," Advances in Applied Ceramics **108**(4), 199–202 (2009).

[49] D. Sen, a. K. Patra, S. Mazumder, and S. Ramanathan, "Pore growth during initial and intermediate stages of sintering in ZrO 2-3 mol% Y2O3 compact: A small-angle neutron scattering investigation," J Alloys Compd **361**(1–2), 270–275 (2003).

[50] O. Bikondoa, "On the use of two-time correlation functions for X-ray photon correlation spectroscopy data analysis," J Appl Crystallogr **50**(2), 357–368 (2017).

[51] B.J. Berne, and R. Pecora, *Dynamic Light Scattering: With Applications to Chemistry, Biology, and Physics* (Dover Publications, New York, 2000).

[52] R. Pecora, editor , *Dynamic Light Scattering* (Springer US, Boston, MA, 1985).

[53] P. Akcora, S.K. Kumar, J. Moll, S. Lewis, L.S. Schadler, Y. Li, B.C. Benicewicz, A. Sandy, S. Narayanan, J. Ilavsky, P. Thiyagarajan, R.H. Colby, and J.F. Douglas, "'Gel-like' Mechanical Reinforcement in Polymer Nanocomposite Melts," Macromolecules **43**(2), 1003–1010 (2010).

[54] R. Hernández, A. Nogales, M. Sprung, C. Mijangos, and T.A. Ezquerra, "Slow dynamics of nanocomposite polymer aerogels as revealed by X-ray photocorrelation spectroscopy (XPCS)," J Chem Phys **140**(2), (2014).

[55] O. Czakkel, and A. Madsen, "Evolution of dynamics and structure during formation of a cross-linked polymer gel," EPL (Europhysics Letters) **95**(2), 28001 (2011).

[56] D. Orsi, L. Cristofolini, G. Baldi, and A. Madsen, "Heterogeneous and Anisotropic Dynamics of a 2D Gel," Phys Rev Lett **108**(10), 105701 (2012).

[57] L. Cipelletti, L. Ramos, S. Manley, E. Pitard, D.A. Weitz, E.E. Pashkovski, and M. Johansson, "Universal non-diffusive slow dynamics in aging soft matter," Faraday Discuss **123**, 237–251 (2003).

[58] F. Augusto de Melo Marques, R. Angelini, E. Zaccarelli, B. Farago, B. Ruta, G. Ruocco, and B. Ruzicka, "Structural and microscopic relaxations in a colloidal glass," Soft Matter **11**(3), 466–471 (2015).

[59] D. Bahadur, Q. Zhang, E.M. Dufresne, P. Grybos, P. Kmon, R.L. Leheny, P. Maj, S. Narayanan, R. Szczygiel, J.W. Swan, A. Sandy, and S. Ramakrishnan, "Evolution of structure and dynamics of thermo-reversible nanoparticle gels—A combined XPCS and rheology study," J Chem Phys **151**(10), (2019).

[60] A. Jain, F. Schulz, F. Dallari, V. Markmann, F. Westermeier, Y. Zhang, G. Grübel, and F. Lehmkühler, "Three-step colloidal gelation revealed by time-resolved x-ray photon correlation spectroscopy," J Chem Phys **157**(18), (2022).

[61] T. Zinn, L. Sharpnack, and T. Narayanan, "Dynamics of magnetic Janus colloids studied by ultra small-angle X-ray photon correlation spectroscopy," Soft Matter **19**(13), 2311–2318 (2023).

[62] Z. Filiberti, R. Piazza, and S. Buzzaccaro, "Multiscale relaxation in aging colloidal gels: From localized plastic events to system-spanning quakes," Phys Rev E **100**(4), 042607 (2019).

[63] L. Cipelletti, and L. Ramos, "Slow dynamics in glassy soft matter," Journal of Physics: Condensed Matter **17**(6), R253–R285 (2005).

[64] J.-P. Bouchaud, and E. Pitard, "Anomalous dynamical light scattering in soft glassy gels," The European Physical Journal E **6**(3), 231–236 (2001).

[65] P.H. Handle, L. Rovigatti, and F. Sciortino, "q-Independent Slow Dynamics in Atomic and Molecular Systems," Phys Rev Lett **122**(17), 175501 (2019).

[66] L. Rovigatti, G. Nava, T. Bellini, and F. Sciortino, "Self-Dynamics and Collective Swap-Driven Dynamics in a Particle Model for Vitrimers," Macromolecules **51**(3), 1232–1241 (2018).

[67] G. Nava, M. Rossi, S. Biffi, F. Sciortino, and T. Bellini, "Fluctuating Elasticity Mode in Transient Molecular Networks," Phys Rev Lett **119**(7), 078002 (2017).

[68] N. Nemoto, A. Koike, and K. Osaki, "Dynamic Light Scattering and Dynamic Viscoelasticity of Poly(vinyl alcohol) in Aqueous Borax Solutions. 2. Polymer Concentration and Molecular Weight Effects," Macromolecules **29**(5), 1445–1451 (1996).

[69] E. Michel, M. Filali, R. Aznar, G. Porte, and J. Appell, "Percolation in a Model Transient Network: Rheology and Dynamic Light Scattering," Langmuir **16**(23), 8702–8711 (2000).

[70] G. Monaco, A. Cunsolo, G. Ruocco, and F. Sette, "Viscoelastic behavior of water in the terahertz-frequency range: An inelastic x-ray scattering study," Phys Rev E **60**(5), 5505–5521 (1999).

[71] R. Angelini, P. Giura, D. Fioretto, G. Monaco, G. Ruocco, and F. Sette, "Microscopic dynamics and relaxation processes in liquid hydrogen fluoride," Phys Rev B **70**(22), 224302 (2004).

[72] A. Martinelli, F. Caporaletti, F. Dallari, M. Sprung, F. Westermeier, G. Baldi, and G. Monaco, "Reaching the Yield Point of a Glass During X-Ray Irradiation," Phys Rev X **13**(4), 041031 (2023).

[73] E. Alfinelli, F. Caporaletti, A. Martinelli, G. Monaco, M. Sprung, and G. Baldi, "Wave vector dependence of x-ray beam induced dynamics in sodium silicate glasses," Phys Rev B **110**(9), 094207 (2024).

[74] A. Jain, F. Schulz, I. Lokteva, L. Frenzel, G. Grübel, and F. Lehmkühler, "Anisotropic and heterogeneous dynamics in an aging colloidal gel," Soft Matter **16**(11), 2864–2872 (2020).

[75] J. Möller, and T. Narayanan, "Velocity Fluctuations in Sedimenting Brownian Particles," Phys Rev Lett **118**(19), 198001 (2017).

[76] H. Guo, S. Ramakrishnan, J.L. Harden, and R.L. Leheny, "Gel formation and aging in weakly attractive nanocolloid suspensions at intermediate concentrations," J Chem Phys **135**(15), (2011).

[77] O. Czakkel, B. Nagy, E. Geissler, and K. László, "Effect of molybdenum on the structure formation of resorcinol–formaldehyde hydrogel studied by coherent x-ray scattering," J Chem Phys **136**(23), (2012).

[78] Y. Chen, S.A. Rogers, S. Narayanan, J.L. Harden, and R.L. Leheny, "Microscopic ergodicity breaking governs the emergence and evolution of elasticity in glass-forming nanoclay suspensions," Phys Rev E **102**(4), 042619 (2020).

[79] A.M. Puertas, M. Fuchs, and M.E. Cates, "Dynamical heterogeneities close to a colloidal gel," J Chem Phys **121**(6), 2813–2822 (2004).

[80] C.J. Dibble, M. Kogan, and M.J. Solomon, "Structural origins of dynamical heterogeneity in colloidal gels," Phys Rev E **77**(5), 050401 (2008).

[81] P. Chaudhuri, Y. Gao, L. Berthier, M. Kilfoil, and W. Kob, "A random walk description of the heterogeneous glassy dynamics of attracting colloids," Journal of Physics: Condensed Matter **20**(24), 244126 (2008).

[82] D. Mangal, G.S. Vera, S. Aime, and S. Jamali, "Small variations in particle-level interactions lead to large structural heterogeneities in colloidal gels," Soft Matter **20**(24), 4692–4698 (2024).

[83] E. Zaccarelli, P.J. Lu, F. Ciulla, D.A. Weitz, and F. Sciortino, "Gelation as arrested phase separation in short-ranged attractive colloid–polymer mixtures," Journal of Physics: Condensed Matter **20**(49), 494242 (2008).

[84] M. Rokita, M. Handke, and W. Mozgawa, "Spectroscopic studies of the amorphous SiO2–AlPO4 materials," J Mol Struct **511–512**, 277–280 (1999).

[85] C.C. de Araujo, L. Zhang, and H. Eckert, "Sol-gel preparation of AlPO4–SiO2 glasses with high surface mesoporous structure," J Mater Chem **16**(14), 1323 (2006).

[86] C. Belver, and M.Á. Vicente, "Porous Silica Gel by Acid Leaching of Metakaolin," in *Materials Syntheses*, (Springer Vienna, Vienna, 2008), pp. 47–51.

[87] M. Lenarda, L. Storaro, A. Talon, E. Moretti, and P. Riello, "Solid acid catalysts from clays: Preparation of mesoporous catalysts by chemical activation of metakaolin under acid conditions," J Colloid Interface Sci **311**(2), 537–543 (2007).

[88] A.K. Panda, B.G. Mishra, D.K. Mishra, and R.K. Singh, "Effect of sulphuric acid treatment on the physico-chemical characteristics of kaolin clay," Colloids Surf A Physicochem Eng Asp **363**(1–3), 98–104 (2010).

[89] J.T. Reiser, J. V. Ryan, and N.A. Wall, "Sol–Gel Synthesis and Characterization of Gels with Compositions Relevant to Hydrated Glass Alteration Layers," ACS Omega **4**(15), 16257–16269 (2019).

[90] C.J. Brinker, and G.W. Scherer, "Sol → gel → glass: I. Gelation and gel structure," J Non Cryst Solids **70**(3), 301–322 (1985).

[91] B. Hammouda, D.L. Ho, and S. Kline, "Insight into clustering in poly(ethylene oxide) solutions," Macromolecules **37**(18), 6932–6937 (2004).

[92] M. Chalal, F. Ehrburger-Dolle, I. Morfin, F. Bley, M.-R. Aguilar de Armas, M.-L. López Donaire, J. San Roman, N. Bölgen, E. Pişkin, O. Ziane, and R. Casalegno, "SAXS Investigation of the Effect of Temperature on the Multiscale Structure of a Macroporous Poly(N -isopropylacrylamide) Gel," Macromolecules **43**(4), 2009–2017 (2010).

[93] A. Meiszterics, and K. Sinkó, "Sol–gel derived calcium silicate ceramics," Colloids Surf A Physicochem Eng Asp **319**(1–3), 143–148 (2008).

[94] L.Y. Sun, R.N. Vasin, A.Kh. Islamov, I.A. Bobrikov, J. Cifre, I.S. Golovin, and A.M. Balagurov, "Influence of spinodal decomposition on structure and thermoelastic martensitic transition in MnCuAlNi alloy," Mater Lett **275**, 128069 (2020).

[95] E.M. Saffer, M.A. Lackey, D.M. Griffin, S. Kishore, G.N. Tew, and S.R. Bhatia, "SANS study of highly resilient poly(ethylene glycol) hydrogels," Soft Matter **10**(12), 1905 (2014).

[96] P. Perez, F. Plieva, A. Gallardo, J. San Roman, M.R. Aguilar, I. Morfin, F. Ehrburger-Dolle, F. Bley, S. Mikhalovsky, I.Yu. Galaev, and B. Mattiasson, "Bioresorbable and Nonresorbable Macroporous Thermosensitive Hydrogels Prepared by Cryopolymerization. Role of the Cross-Linking Agent," Biomacromolecules **9**(1), 66–74 (2008).

[97] A. Viani, and P. Mácová, "Polyamorphism and frustrated crystallization in the acid-base reaction of magnesium potassium phosphate cements," CrystEngComm **20**(32), (2018).

[98] A. Viani, G. Mali, and P. Mácová, "Investigation of amorphous and crystalline phosphates in magnesium phosphate ceramics with solid-state 1H and 31P NMR spectroscopy," Ceram Int **43**(8), 6571–6579 (2017).

[99] S. Jungblut, J.-O. Joswig, and A. Eychmüller, "Diffusion- and reaction-limited cluster aggregation revisited," Physical Chemistry Chemical Physics **21**(10), 5723–5729 (2019).

[100] A.C. da Silva, "Structure and Percolation of Bioglasses," in *Biocompatible Glasses: From Bone Regeneration to Cancer Treatment*, edited by J. Marchi, (Springer, 2016), pp. 49–84.

[101] C. Le Losq, D.R. Neuville, W. Chen, P. Florian, D. Massiot, Z. Zhou, and G.N. Greaves, "Percolation channels: a universal idea to describe the atomic structure and dynamics of glasses and melts," Sci Rep **7**(1), 16490 (2017).

[102] M.I. Ojovan, "The Modified Random Network (MRN) Model within the Configuron Percolation Theory (CPT) of Glass Transition," Ceramics **4**(2), 121–134 (2021).

[103] H. Tsurusawa, M. Leocmach, J. Russo, and H. Tanaka, "Direct link between mechanical stability in gels and percolation of isostatic particles," Sci Adv **5**(5), (2019).